Terahertz radiation sources with an active region based on super-multiperiod AlGaAs/GaAs superlattices

© A.S. Dashkov[1,2], L.G. Gerchikov[1,3], L.I. Goray[1,2,4,5], N.A. Kostromin[2,3], A.D. Bouravleuv[2,4,5]

[1] Alferov Federal State Budgetary Institution of Higher Education
and Science Saint Petersburg National Research Academic University of the Russian Academy of Sciences,
194021 St. Petersburg, Russia
[2] St. Petersburg State Electrotechnical University „LETI“,
197022 St. Petersburg, Russia
[3] Peter the Great Saint-Petersburg Polytechnic University,
195251 St. Petersburg, Russia
[4] Institute of Analytical Instrument Making Russian Academy of Sciences,
198095 St. Petersburg, Russia
[5] Autonomous Non-profit Organization of Higher Education
„University Under Interparlamentary Assembly Of EURASEC“,
199106 St. Petersburg, Russia

E-mail: dashkov.alexander.om@gmail.com

Received May 5, 2023
Revised June 29, 2023
Accepted July 6, 2023

In this article, several designs of the active region of the THz radiation source are considered, taking into account grown super-multiperiod AlGaAs/GaAs superlattices. For the proposed designs, the principal device characteristics are computed: energy band diagram, gain spectrum, and transport characteristics. Based on the calculation results, the authors proposed an optimal design of the active region of a tunable THz radiation source.

Keywords: super-multiperiod superlattice, light amplifiers, terahertz range, finite elements method, gain estimation.

DOI: 10.21883/0000000000

1. Introduction

The terahertz (THz) frequency range has numerous applications in various fields of science and technology, which makes it one of the most promising research objects. In particular, one of the most common applications is THz spectroscopy [1–4], which is used, for example, in security systems for the detection of explosives and prohibited substances [5] and for the control of product quality in production [6]. It also finds its application in medical diagnostics [7], in the creation of broadband communication channels for high-speed information transfer [8].

Nevertheless, this frequency range still remains the least studied, and sources of this range are still in a high demand [1]. This is mainly due to the lack of compact, adjustable and sufficiently powerful THz radiation sources and highly sensitive and low-inertia coherent or broadband receivers operating at room temperature. Therefore, the development of new designs of THz sources is an important scientific task [9]. To replace the common design of the active region based on quantum cascades, the authors propose designs of emitters based on super-multiperiod (SMP) AlGaAs/GaAs superlattices (SL) [10–12]. It is expected that the proposed design can be the basis for development of adjustable THz sources, which are less susceptible to temperature degradation.

2. Active region design

In the case of superlattices, radiation is the result of intersubband electronic transitions between levels of Wannier-Stark ladders through several lattice periods when a voltage is applied. The radiation is amplified due to a large number of periods (about a hundred or more). In this case, the frequency of such a transition is controlled by the magnitude of the applied voltage, and the presence of a set of transitions through a different number of periods makes it possible to adjust the radiation frequency in a wide range.

In this study, the SL parameters were selected so that several requirements were met at once: at least two (preferably exactly two) energy levels are formed in the quantum well, the energy gap between them exceeds the radiation energy; the energy of the electronic transition over several periods corresponds to the THz range; the structure contains a set of such THz transitions, which allows tuning the radiation frequency; the position of the levels in the well is chosen so as to reduce the probability of electronic transitions inside the well.

Parameters of the proposed structures are given in Table 1. The doping concentration for all the above structures was $10^{16}\,\mathrm{cm}^{-3}$. For each of the structures, fan energy diagrams were calculated (Figure 1), which demonstrated a set of the desired transitions in the THz range. For example, for SL3 the transition energies of such a set are 2.8, 4.7, and

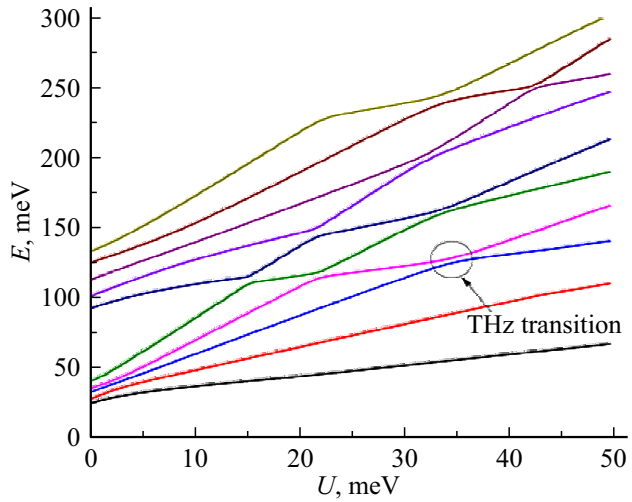

Figure 1. Dependence of the position of energy electronic levels E on the applied voltage U for one period for SL3. (The colored version of the figure is available on-line).

Table 1. Parameters of studied SLs

Identification	Composition	Layer thicknesses, nm
SL1	GaAs/$Al_{0.2}Ga_{0.8}As$	10/2
SL2	GaAs/$Al_{0.3}Ga_{0.7}As$	12.9/2
SL3	GaAs/$Al_{0.35}Ga_{0.65}As$	12.6/1.5
SL4	GaAs/$Al_{0.3}Ga_{0.7}As$	7/2

8.3 meV (0.7, 1.1, and 2 THz, respectively). The presence of such a set of transitions is a necessary condition for creating a tunable radiation source.

3. Calculation methods

The electron and hole energy spectra, gain spectra, and transport characteristics were calculated for the proposed designs using analytical models and numerical modeling methods. In particular, the positions of discrete electron and hole levels of the structures were obtained by numerically solving the stationary Schrödinger equation using the finite elements method [13,14] in the effective mass approximation [15,16]. The $E(k)$ dependence was obtained using the Kronig-Penney model in the strong coupling approximation [17–19]. Effective hole masses were calculated on the basis of Luttinger parameters [20,21]. The gain spectrum and the loss level were determined by numerically solving the Helmholtz equation for the classical waveguide structure [22,23]. To verify the hypothesis of the absence of negative differential conductivity (NDC) regions [24], estimations of current-voltage curves (IV-curves) were carried out. The obtained theoretical dependences were calculated using the numerical Monte Carlo method taking into account the scattering of carriers by longitudinal optical (LO) phonons [13].

4. Experimental samples

For the calculated structures, experimental samples were grown using the molecular beam epitaxy (MBE) method. Previously, for a number of similar structures, including the SL1 structure, the structural perfection of layers was studied using the methods of X-ray reflectometry and diffractometry [25]. The results of these studies showed a high structural perfection of the grown SMP-structures and insignificant deviations in layer thicknesses and interface roughness [25–27]. Also, photoluminescence (PL) spectra were obtained for a number of structures [26]. The position of PL peaks corresponds with satisfactory accuracy to the position of the levels obtained using numerical modeling methods.

5. Results of numerical calculations

For the structures considered in this study, the dependences of the gain on the applied voltage were first calculated (Figure 2). The calculation results showed that the gain for all the structures exceeds the estimated losses in waveguide $\alpha_{loss} \approx 60\,cm^{-1}$.

In addition to the position of electronic energy levels, the position of the levels of heavy and light holes, as well as the broadening of each energy level, were calculated for all structures (Table 2, Figure 3). In the future, this data can be used for a detailed experimental study of SL samples using the photoreflection method [28,29].

The results obtained are indicative of the fact that when creating SLs with rather wide QWs (thickness > 10 nm), the emergence of the third unwanted electronic level is observed, and in some cases also the emergence of hole levels takes place. A similar situation is observed for the SL2 structure (well thickness is 12.9 nm): three electronic levels are formed in it as well. In this case, the two-level model

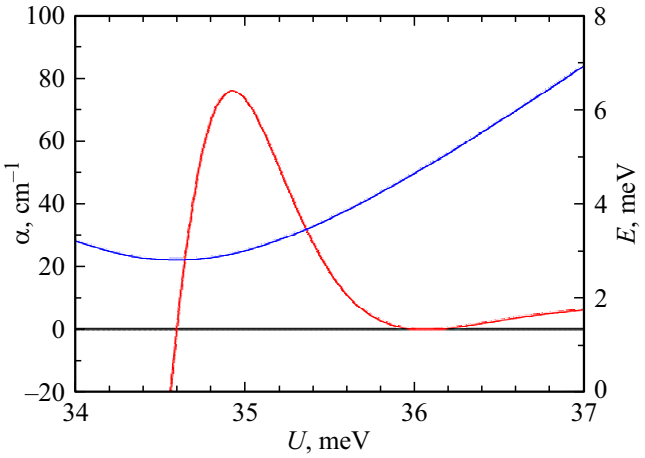

Figure 2. Dependence of the gain and transition energy on the applied voltage U over one period for the proposed active region design of SL3.

Table 2. Position and width of electron and hole minibands in the conduction band and valence band for SLs from Table 1

Identification of the level	Position relative to the SL3 well bottom, meV	Width of the level for SL3, meV	Position relative to the SL4 well bottom, meV	Width of the level for SL4, meV
e_1	24	1	60	7
e_2	92	8	211	31
e_3	208	17	–	–
hh_1	5	1	14	1
hh_2	21	2	56	5
hh_3	48	9	123	24
lh_1	19	1	42	8
lh_2	74	30	–	–
lh_3	–	–	–	–

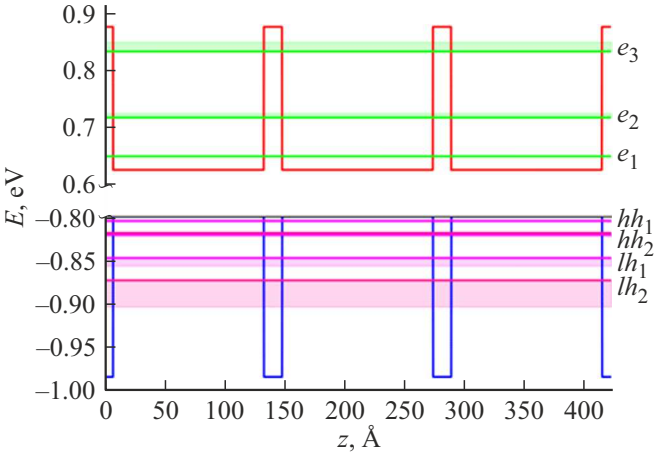

Figure 3. Energy diagram for SL3.

no longer works and the generation effect predicted earlier in [30] for similar structures cannot be effectively realized.

For thin wells (thickness < 8 nm), it can be said that there is only one electronic level, which makes inapplicable the two-level model again. This negative effect arises due to the fact that in narrow QWs the upper (the 2-th) energy level in SLs is actually bound to the continuum. The calculation results for the SL1 structure show the presence of only two electronic levels. Thus, SL1 is an intermediate and optimal structure from the point of view of the number of electronic levels and the applicability of the two-level model [30].

Another important fact established in the process of calculations is the magnitude of the broadening of energy levels: for the lowest energy levels, the broadening is of the order of a few meV, which is acceptable for the implementation of THz generation. In this case, the broadening of the third level exceeds 10 meV.

When implementing a radiation source, it is also important to take into account the paths of nonradiative relaxation of carriers. In particular, the relaxation of electrons on LO phonons during transitions between levels in the SL. To assess the effect of this scattering factor, the relaxation times from the second electronic level to the first electronic level, as well as the transition times from these two levels to others within three periods, were calculated. To visually represent the results, we calculated the quantity usually introduced to evaluate the efficiency of radiation sources, in particular quantum cascade lasers [13]:

$$F_M = D_{ul}^2 \cdot \tau_{\text{eff}} = D_{ul}^2 \cdot \tau_u \left(1 - \frac{\tau_l}{\tau_{ul}}\right), \qquad (1)$$

where D_{ul} is dipole matrix element of the lasing transition, τ_i is nonradiative relaxation time from the i level. The given value allows us to simultaneously take into account both the magnitude of the dipole matrix element and the population inversion of the levels $\Delta n \sim \tau_{\text{eff}}$.

Results of the calculation show that structures with narrower wells make it possible to significantly increase F_M by increasing the level of population inversion. For the dipole matrix element such a pronounced dependence is not observed. This effect can be associated with several facts:

– in narrower wells a smaller number of energy levels is observed, i. e. transitions occur between fewer levels;

– carriers in narrower wells are localized inside the wells to a greater extent, i. e. the integral of the probability

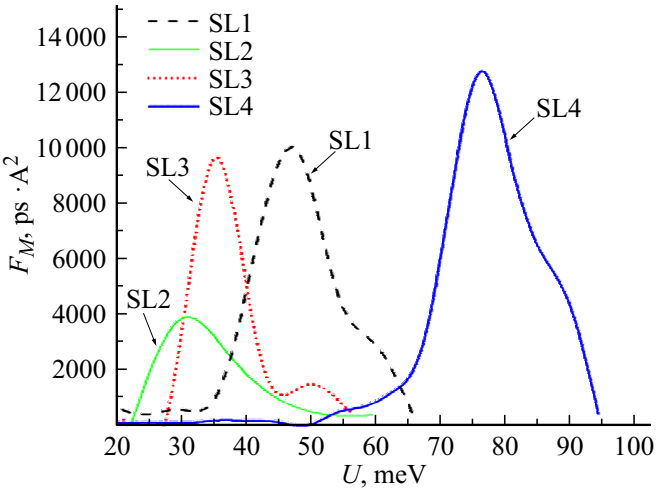

Figure 4. Calculated values F_M for SLs from Table 1 in the vicinity of the main THz transition point.

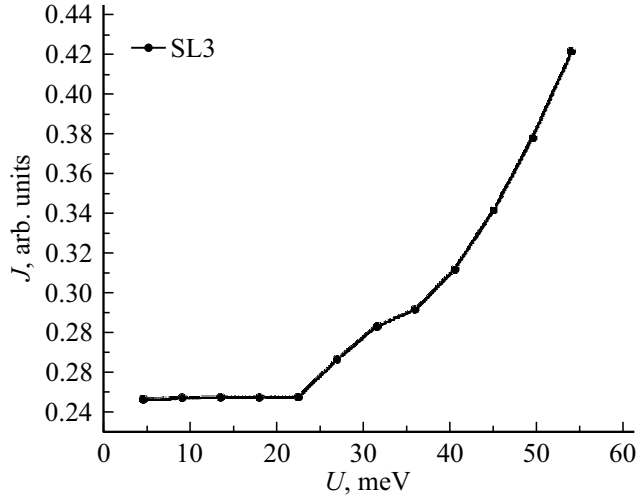

Figure 5. IV-curve obtained as a result of numerical modeling of SL3 in the vicinity of the point of the main THz transition.

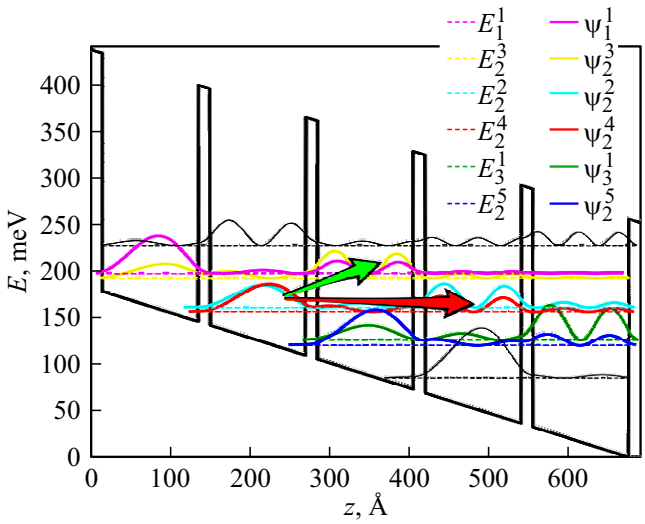

Figure 6. Energy diagram of the conduction band profile and results of the numerical solving of the Schrödinger equation (energy levels and wave functions) at $U = 32$ meV. The superscript is responsible for the numbering of the wells, the subscript indicates position of the level inside the well. The red arrow indicates the radiative transition, the green arrow indicates the diagonal transition providing the positive differential conductivity.

density of an electron being inside the well is larger for narrower wells.

Previously, the value of the differential conductivity in the region near the radiative transition was estimated for SL1. The relaxation times for electronic levels calculated in [30] were used in this study in the Monte Carlo method to obtain an estimate of the IV-curve (Figure 5). The obtained dependence does not show the presence of an undesirable effect of the NDC formation, which prevents the generation of radiation.

The observed increase in current density with increasing voltage is explained by the diagram of the radiating transition shown in Figure 6. Before reaching the operating point ($U < 35$ meV), as the voltage increases, the levels between which the radiative transition occurs come closer to each other, and the transition occurs from the 1st level in well n to the 2nd level in well $n + 2$. After the operating point is passed, the mechanism of current increase can be explained by tunneling into well $n + 1$, i.e. by the diagonal transition.

A similar situation can be expected for other operating points, for example, for the radiative transition from well n to well $n + 3$; a diagonal transition to well $n + 2$ will ensure an increase in current. A similar mechanism for creating positive differential conductivity was considered earlier for similar SLs using the method of non-equilibrium Green's functions [31].

6. Conclusion

Thus, in this study designs of the active region based on AlGaAs/GaAs superlattices were presented and theoretically investigated. The authors conducted a series of numerical experiments to model the energy spectrum of charge carriers, gain spectra, current-voltage curves and estimate the parameters of radiation amplification in the considered radiative configurations. Similar experimental structures were grown by molecular beam epitaxy and then studied by photoluminescence methods. The previously obtained experimental spectra demonstrate satisfactory agreement with the presented calculations.

To select the best a comparison among the designs was performed based on the energy diagram, the dipole matrix element and the level of the population inversion. As a result of this comparison, it was found that the optimal thickness of the quantum well layer in the range of 8–10 nm for $Al_{0.3}Ga_{0.7}As$ barrier layers. The analysis of the calculated current-voltage curve has shown the absence of a region of negative differential conductivity for the structure with narrow barriers (1–1.5 nm).

Funding

The study was supported by the Ministry of Education and Science of the Russian Federation within the experimental research activities („youth laboratory“ state assignment No. 075-01438-22-06, FSEE-2022-0018) and the Russian Science Foundation within the theoretical research activities (RSF 23-29-00216).

Conflict of interest

The authors declare that they have no conflict of interest.

References

[1] N.V. Kinev, K.I. Rudakova, L.V. Filippenko, V.P. Koshelets, FTT, **63** (9), 1204 (2021) (in Russian).
[2] S.L. Dexheimer. *Terahertz Spectroscopy: Principles and Applications* (N.Y., CRC Press, 2008) p. 360.
[3] M.C. Beard, G.M. Turner, C.A. Schmuttenmaer. J. Phys. Chem. B, **106** (29), 7146 (2002).
[4] J.B. Baxter, G.W. Guglietta. Anal. Chem., **83** (12), 4342 (2011).
[5] A.G. Davies, A.D. Burnett, W. Fan, E.H. Linfield, J.E. Cunningham. Materials Today, **11** (3), 18 (2008).
[6] J. True, C. Xi, N. Jessurun, K. Ahi, N. Asadizanjani. Opt. Eng., **60** (6), 060901 (2021).
[7] M.O. Mattsson, M. Simkó. Med. Devices (Auckl.), **12**, 347 (2019).
[8] K. Tekbiyik, A.R. Ekti, G.K. Kurt, A. Gorcin. Phys. Commun., **35**, 100700 (2019).
[9] A. Khalatpour, A.K. Paulsen, C. Deimert, Z.R. Wasilewski, Q. Hu. Nature Photonics, **15**, 16 (2021).
[10] A.A. Andronov, A.V. Ikonnikov, K.V. Maremianin, V.I. Pozdnjakova, Y.N. Nozdrin, A.A. Marmalyuk, A.A. Padalitsa, M.A. Ladugin, V.A. Belyakov, I.V. Ladenkov, A.G. Fefelov. J. Semiconductors, **52**, 431 (2018).
[11] A.A. Andronov, E.P. Dodin, D.I. Zinchenko, Yu.N. Nozdrin, M.A. Ladugin, A.A. Marmalyuk, A.A. Padalitsa, V.A. Belyakov, I.V. Ladenkov, A.G. Fefelov. JETP Lett., **102**, 207 (2015).
[12] A.A. Andronov, I.M. Nefedov, A.V. Sosnin. J. Semiconductors, **37**, 360 (2003).
[13] C. Jirauschek, T. Kubis. Appl. Phys. Rev., **1** (1), 011307 (2014).
[14] P. Harrison, A. Valavanis. *Quantium wells, wires and dots: theoreticall and computation physics of semiconductor nanostructure* (West Sussex, UK: Hoboken, NG: John Wiley & Sons, Inc., 2016) p. 624.
[15] A.S. Dashkov, L.I. Goray. J. Phys.: Conf. Ser., **1410**, 012085 (2019).
[16] A.S. Dashkov, L.I. Goray. J. Semiconductors, **54**, 1823 (2020).
[17] V.E. Gasumyants, D.A. Firsov, *Elektrony i fonony v kvantorazmernykh sistemakh* (SPb., Izd-vo Politekhn. un-ta, 2008) p. 96. (in Russian).
[18] H.S. Cho, P.R. Prucnal. Phys. Rev. B, **36**, 3237 (1987).
[19] F. Szmulowicz. Eur. J. Phys., **18** (5), 392 (1997).
[20] A.Yu. Egorov. Avtoref. dokt. dis. (SPb, SPbAU RAN, 2011). (in Russian).
[21] I. Vurgaftman, J.R. Meyer. J. Appl. Phys., **94** (6), 3675 (2003).
[22] B.S. Williams. Synopsis of the dissertation of M. S. in EECS (Cambridge, Massachusetts, MIT, 1998).
[23] H. Kogelnik. *Theory of optical waveguides* (Heidelberg, Springer Verlag, 1988) p. 82.
[24] A.A. Andronov, E.P. Dodin, D.I. Zinchenko, Yu.N. Nozdrin, FTP, **43** (2), 248 (2009). (in Russian).
[25] L.I. Goray, E.V. Pirogov, M.S. Sobolev, N.K. Polyakov, A.S. Dashkov, M.V. Svechnikov, A.D. Buravlev, ZhTF, **90** (11), 1906 (2020). (in Russian).
[26] L.I. Goray, E.V. Pirogov, M.S. Sobolev, N.K. Polyakov, A.S. Dashkov, M.V. Svechnikov, A.D. Buravlev, Pisma ZHTF, **47** (15), 7 (2021). (in Russian).
[27] L. Goray, E. Pirogov, M. Sobolev, I. Ilkiv, A. Dashkov, E. Nikitina, E. Ubyivovk, L. Gerchikov, A. Ipatov, Y. Vainer, M. Svechnikov, P. Yunin, N. Chkhalo, A. Bouravlev. J. Phys. D: Appl. Phys., **53**, 455103 (2020).
[28] D.S. Smotrin, N.V. Baidus, A.A. Bryukov, O.S. Komkov, O.E. Gordyushenkov. *Tez. dokl. XIX Mezhd. simp. „Nanofizika i nanoelektronika“* (N. Novgorod, Russia, 2012), v. 2, p. 388. (in Russian).
[29] V.D. Goryacheva, M.S. Mironova, O. S. Komkov. J. Phys.: Conf. Ser., **1038**, 012124 (2018).
[30] L.G. Gerchikov, A.S. Dashkov, A.D. Buravlev, ZhETF **160** (2), 197 (2021). (in Russian).
[31] D.O. Winge, M. Franckié, A. Wacker. AIP Advances, **6** (4), 045025 (2016).

Translated by Y.Alekseev